

(sub)GeV Dark Matter in the $U(1)_X$ Higgs Portal Model

Amir Amiri*, Bastián Díaz Sáez†, Karim Ghorbani*

**Physics Department, Faculty of Sciences, Arak University, Arak 38156-8-8349, Iran*

†Departamento de Física, Universidad de Santiago de Chile, Casilla 307, Santiago, Chile

Abstract

In this research we consider a $U(1)_X$ gauge boson acting as a dark matter candidate. The vector dark matter gets mass when a complex singlet scalar breaks the gauge symmetry spontaneously. The dark matter candidates communicate with the SM particles via a scalar-Higgs portal. The focus in this work is on the dark matter mass smaller than 10 GeV. This parameter space is not studied thoroughly before. Dark matter annihilation via forbidden channel and near pole are studied in order to place constraints from observed relic density and CMB. Other bounds from colliders, beam-dump experiments, and astrophysical observations are imposed. Taking into account all the bounds including the direct detection upper limits, the viable space is achieved.

1 Introduction

The weakly interacting massive particles (WIMPs) as dark matter (DM) candidates come in various types of interactions with the normal matter [1–3]. Recent improvements on the direct detection (DD) experiments have been able to exclude a large portion of the parameter space in minimal extensions of the Standard Model (SM). The minimal extensions are used to be applied in both simplified DM models and in effective field theory (EFT) DM models. The disadvantage of the latter approach is that the viable parameter space is shrunk by the constraints from the applicability criterion of the EFT models [4].

A generic question is that how small the WIMP mass might be when assuming a thermal mechanism for the production of dark matter. We address this issue in the present work within a $U(1)_X$ vector DM model. The model consists of a dark gauge boson acting as a DM candidate and a complex scalar which is responsible for the spontaneous breaking of the gauge symmetry and thereby giving mass to the dark matter candidate. DM particles can communicate with the normal matter via scalar-Higgs portal. The abelian vector DM model is studied earlier [5–14]. In all the previous works, points in the parameter space with quite small singlet scalar mass and at the same time very small mixing angle are not considered.

Moreover, we study the parameter space respecting the observed relic density and upper bounds on the annihilation cross section from Cosmic Microwave Background (CMB). To address this issue, one has to consider the forbidden and near pole annihilation channels carefully. There are also various constraints from collider searches, beam-dump experiments, and astrophysical observations, which are incorporated in this work.

The paper has the following structure. The DM model is described in the next section along with theoretical bounds on the couplings from vacuum stability. Focusing on the low mass DM we present the relevant Feynman diagrams for the DM annihilation and study the behavior of the DM relic density in section making use of MicrOMEGAs code³. Bounds from CMB and observed relic density on the DM annihilation are studied simultaneously in 4. We summarize all the relevant experimental and astrophysical bounds in section 6. The elastic scattering of DM off the proton is obtained in section 5 and the viable parameter is found after imposing all the constraints. Finally, a formula for the DM self-scattering cross section is achieved in section ?? followed by discussions. The conclusion is provided by section 8. In the Appendix we provide the DM annihilation cross sections.

2 Model

We consider a model as a minimal extension to the SM with a new $U(1)_X$ gauge symmetry introducing a complex scalar field, S , in the following Lagrangian

$$\mathcal{L}_{\text{DM}} = (\mathcal{D}_\mu S)(\mathcal{D}^\mu S)^* - \frac{1}{4}X^{\mu\nu}X_{\mu\nu} - \mathcal{V}(S, H), \quad (1)$$

where the covariant derivative is $\mathcal{D}_\mu = \partial_\mu - i\alpha_X q_X X_\mu$, in which α_X is the gauge coupling and q_X is the $U(1)_X$ charge of the corresponding field which is taken unity. The strength field tensor for the gauge field X_μ is given by $X_{\mu\nu} = \partial_\mu X_\nu - \partial_\nu X_\mu$. The scalar potential entailing the Higgs portal is

$$\mathcal{V}(S, H) = \mu_H |H|^2 + \lambda_H |H|^4 + m^2 |S|^2 + \lambda_S |S|^4 + \lambda_{HS} |S|^2 |H|^2. \quad (2)$$

The Lagrangian enjoys an additional *charge conjugation* symmetry

$$X^\mu \rightarrow -X^\mu, \quad S \rightarrow S^*. \quad (3)$$

When the complex scalar gets a nonzero expectation value this breaks the gauge symmetry spontaneously, after which the remaining residual symmetry for the vector gauge boson is $X^\mu \rightarrow -X^\mu$. The parametrization of the complex scalar field around its vacuum is

$$S = \left(\frac{v_s + \phi_1}{2} \right) e^{-i\phi_2/v_s}, \quad (4)$$

here ϕ_1 and ϕ_2 are real scalar fields. It is possible to gauge away the Goldstone field ϕ_2 and rendering the massless gauge boson massive, such that $m_X = v_s \alpha_X$. On the other hand, the Higgs doublet takes a vacuum expectation value, v_h , and in unitary gauge we write down the Higgs field as $H = (0 \ v_h + h_1)^T / \sqrt{2}$. Plugging the Higgs doublet and singlet scalar in the Lagrangian and after some simplification we arrive at the following interaction terms,

$$\begin{aligned} \mathcal{L}_{int} = & \alpha_X^2 v_s X_\mu X^\mu \phi_1 + \frac{1}{2} \alpha_X^2 X_\mu X^\mu \phi_1^2 - \frac{1}{4} \lambda_S \phi_1^4 - \lambda_S v_s \phi_1^3 - \frac{1}{4} \lambda_H h_1^4 - \lambda_H v_h h_1^3 \\ & - \frac{1}{2} \lambda_{HS} v_h h_1 \phi_1^2 - \frac{1}{2} \lambda_{HS} v_s h_1^2 \phi_1 - \frac{1}{4} \lambda_{HS} h_1^2 \phi_1^2. \end{aligned} \quad (5)$$

The scalar mass matrix is also obtained as

$$\mathcal{M}^2 = \begin{pmatrix} 2\lambda_S v_s^2 & \lambda_{HS} v_h v_s \\ \lambda_{HS} v_h v_s & 2\lambda_H v_h^2 \end{pmatrix}. \quad (6)$$

A scalar field transformation is needed in order to diagonalize the mass matrix. Therefore, the physical or mass eigenstates, h are ϕ , are defined in terms of the mixing angle ϵ ,

$$h = h_1 \cos(\epsilon) + \phi_1 \sin(\epsilon), \quad \phi = -h_1 \sin(\epsilon) + \phi_1 \cos(\epsilon), \quad (7)$$

where the mixing angle is given by the relation,

$$\tan(2\epsilon) = \frac{2v_h v_s}{m_h^2 - m_\phi^2} \lambda_{HS}, \quad (8)$$

with m_h and m_ϕ the physical masses of the SM Higgs and the singlet scalar, respectively. The quartic couplings are obtained in terms of the mixing angle and the physical scalar masses

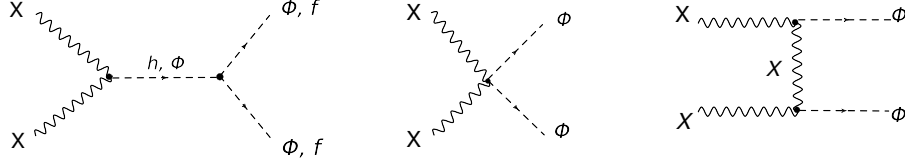


Figure 1: The relevant Feynman diagrams for the vector dark matter annihilation with mass smaller than ~ 10 GeV. The diagram in the left is a s -channel annihilation process and the process shown in the right side takes place in both t - and u -channel.

$$\begin{aligned}
\lambda_H &= \frac{1}{2v_h^2} (m_h^2 \cos^2 \epsilon + m_\phi^2 \sin^2 \epsilon), \\
\lambda_S &= \frac{1}{2v_s^2} (m_h^2 \sin^2 \epsilon + m_\phi^2 \cos^2 \epsilon), \\
\lambda_{HS} &= \frac{\sin 2\epsilon}{4v_h v_s} (m_\phi^2 - m_h^2).
\end{aligned} \tag{9}$$

We will impose the conditions by which the Higgs potential remains bounded from below. These conditions read

$$\lambda_H > 0, \quad \lambda_S > 0, \quad \lambda_{HS} > -2\sqrt{\lambda_H \lambda_S}. \tag{10}$$

Also, satisfying the relations in Eq. 10 warrants the electroweak vacuum to be a global minimum [6]. The free parameters in this model are m_X, m_ϕ, ϵ , and α_X .

3 Relic Density from Thermal Freeze-out

Assuming DM is in thermal equilibrium in the early times, dark matter production is then happening at temperatures very smaller than the DM mass when it goes out of equilibrium, the so-called freeze-out mechanism of dark matter particles. The freeze-out temperature, T_f , depends on the DM annihilation cross section and DM mass. The Boltzmann equation describes how the DM number density, n_X , evolves in an expanding Universe,

$$\dot{n}_X + 3\mathcal{H}n_X = -\langle\sigma_{\text{ann}}v_{\text{rel}}\rangle[n_X^2 - (n_X^{\text{eq}})^2], \tag{11}$$

where \mathcal{H} is the Hubble parameter, $n_X^{\text{eq}} \sim (m_X T)^{3/2} e^{-m_X/T}$ is the particle density before particles get out of equilibrium, and the thermal average annihilation cross section times the relative velocity is given by

$$\langle\sigma_{\text{ann}}v_{\text{rel}}\rangle = \frac{1}{8m_X^4 T K_2^2(\frac{m_X}{T})} \int_{4m_X^2}^{\infty} ds (s - 4m_X^2) \sqrt{s} K_1\left(\frac{\sqrt{s}}{T}\right) \sigma_{\text{ann}}(s). \tag{12}$$

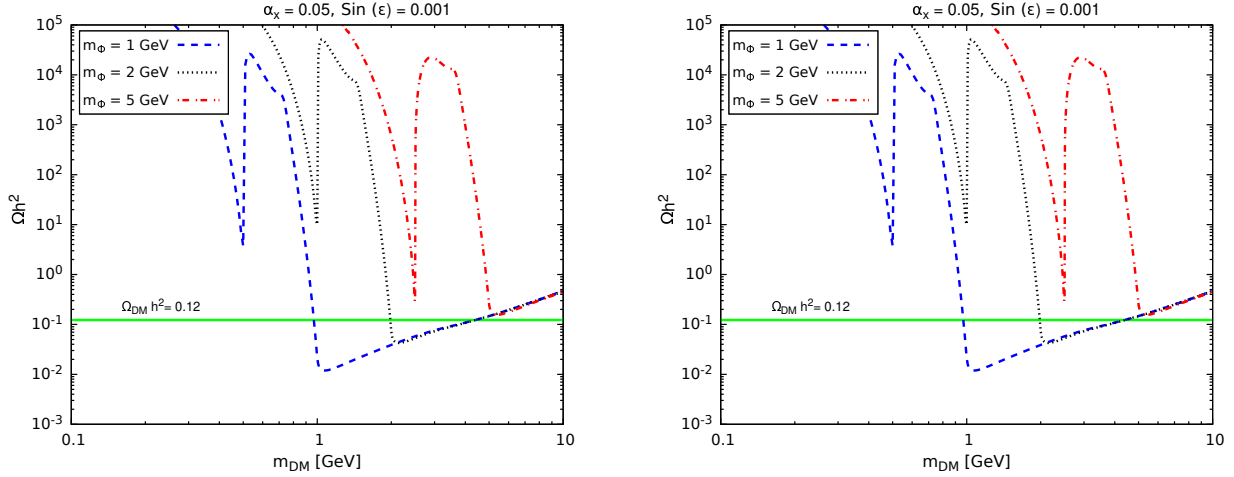


Figure 2: Shown are relic density as a function of DM mass for the gauge coupling $\alpha_X = 0.05$. In the left panel we take the mixing angle such that $\sin \epsilon = 0.001$ and in the right panel we fix it as $\sin \epsilon = 0.01$. The observed DM relic density is shown as a horizontal line at $\Omega h^2 \sim 0.12$.

In the present work DM with mass smaller than ~ 10 GeV annihilates through three different ways diagrammatically as depicted in Fig. 2: 1) A s -channel annihilation process into singlet scalars and the SM fermions as $XX \rightarrow \phi\phi, f\bar{f}$ with mediators being the SM Higgs or the singlet scalar. 2) A contact interaction of DM with the singlet scalars. 3) DM annihilation to singlet scalars via t - and u -channels, with the vector DM acting as the mediator.

It is worth mentioning that the lower limit for a thermal WIMP with $2 \rightarrow 2$ s-wave annihilation to visible final states is found to be about 20 GeV [15]. However, since in the present work we consider the forbidden channels and the resonance effect this lower bound is relaxed. This model is first implemented in the package LanHEP [16] in order to obtain the possible vertices and then the code micrOMEGAs [17] is applied to compute the relic density numerically. First, it is interesting to see the variation of the relic density as a function of DM mass for three different singlet scalar masses $m_\phi = 1, 2, 5$ GeV. To do that we fix the gauge coupling at a reasonable value $\alpha_X = 0.05$. The results are shown for two distinct mixing angles $\sin \epsilon = 0.001$ and $\sin \epsilon = 0.01$ in Fig. 2. It is evident from the two plots with different mixing angles that the relic density behaves almost similarly near the observed relic density, although the bigger ϵ the bigger is the annihilation cross section, and in turn lower relic abundance. It is also apparent from the figures that the relic density is decreasing when the DM mass approaches the singlet scalar mass. The reason for this behavior relies on the fact that when $m_{\text{DM}} \sim m_\phi$, the annihilation channel $XX \rightarrow \phi\phi$ opens up and its cross section increases leading to a reduction of the relic density. When $m_{\text{DM}} < m_\phi$ the annihilation channel $XX \rightarrow f\bar{f}$ is open, and in case m_{DM} is just slightly smaller than m_ϕ then the forbidden channel is also open [18]. In summary, we can conclude that in the low mass region and away from the resonance, the computed relic density complies with the observed value when the singlet scalar mass is $m_\phi \sim m_{\text{DM}}$. The analytical

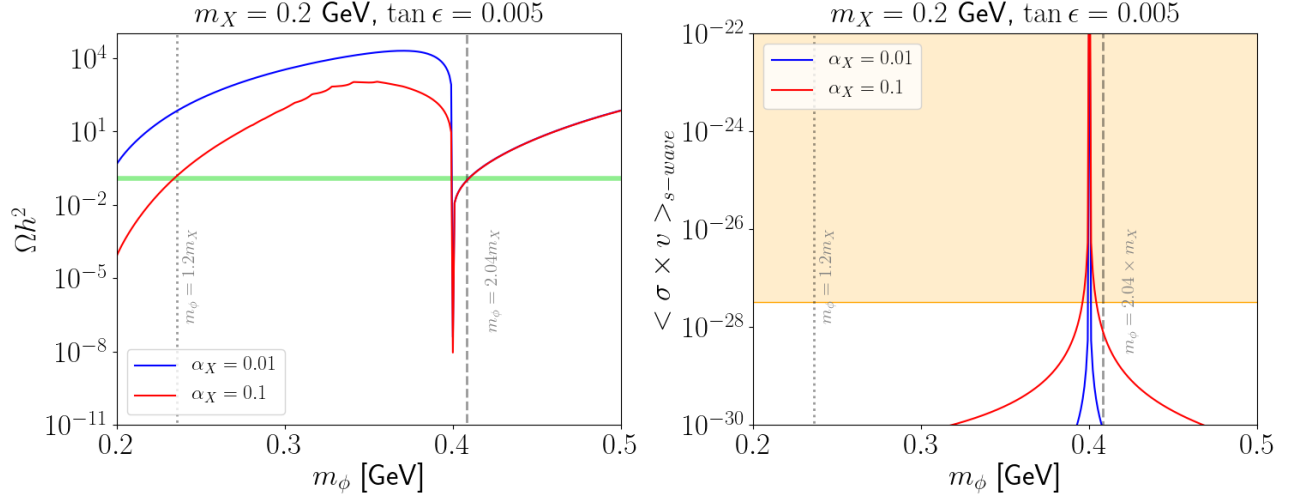


Figure 3: In the *left plot* we show the relic density as a function of the singlet scalar, and in the *right plot* the s -wave annihilation cross section times the velocity as a function of the singlet scalar mass. In both plots we set the DM mass at 0.2 GeV and $\tan \epsilon = 0.005$, with $\alpha_X = 0.1, 0.01$ shown in red and blue, respectively. The observed DM relic density is shown as a horizontal green line at $\Omega h^2 \sim 0.12$ in the left plot, and in the plot in the right we show the CMB bounds as the yellow colored region. The vertical lines in each plot are explained in the text.

formulas for the annihilation cross sections are available in the Appendix. In the analysis in the next sections we constrain the model parameter space by imposing the observed DM relic density, $\Omega_{\text{DM}} = 0.1198 \pm 0.0012$ [19, 20].

4 CMB Bounds

Light dark matter annihilation being a s -wave process in our scenario, can modify the recombination history by injecting energy into the universe. The anisotropies of the CMB is measured very accurately by Planck [19], and this will put strong indirect constraint on the DM annihilation. The upper limit on the DM annihilation at the recombination is given by

$$\frac{f_{\text{eff}}}{m_{\text{DM}}} \langle \sigma v \rangle_{\text{rec}} < 3.2 \times 10^{-28} \text{ cm}^3 \text{ s}^{-1} \text{ GeV}^{-1}, \quad (13)$$

where f_{eff} is an efficiency factor depending on the energy of injected electrons and photons. The efficiency factor for models with s -wave annihilation is computed in [21] as a function of DM mass, and can be applied to any DM model by weighting their results considering the annihilation product. In our analysis for DM mass below 10 GeV, we take $f_{\text{eff}} = 0.1$. At first sight, it might look impossible to reconcile the thermal relic density of about $3 \times 10^{-26} \text{ cm}^3 \text{ s}^{-1}$

to the CMB limits for DM particles with s -wave annihilation and masses below 10 GeV. As discussed in [18,22], there are kinematical regions in the annihilation processes where the s -wave annihilation is not dominating. This happens in two ways. When Boltzmann distributed DM is slightly lighter than the mediator mass, it can dominantly annihilates to the heavier states, the so-called forbidden channels. Another avenue in which higher partial waves dominate is DM annihilation near pole. We proceed by computing the annihilation cross section times the velocity at the recombination era, $\langle\sigma v\rangle_{s\text{-wave}}$. As shown in Fig. 3 for some benchmark points, it is possible to respect the observed relic density and CMB bounds via forbidden channel as $m_\phi/m_{\text{DM}} = 1.20$, and near the pole as $m_\phi/m_{\text{DM}} = 2.04$, for $\tan\epsilon = 0.005$, $m_{\text{DM}} = 0.2$ GeV and $\alpha_X = 0.1$ (we show the blue curve as another point just for comparison, in which it does not fulfill the relic abundance constraint, but the CMB bounds near the pole does). In particular, in the plot in the left shows the red curve intersecting the green horizontal line (correct relic abundance), and both intersection points in the plot in the right are well below the yellow region, which represents the CMB bounds imposed by Eq. 13.

5 Direct Detection Bounds

We consider direct detection bounds on the elastic scattering of DM off the proton from three experiments, Xenon1T [23], DarkSide50-S2 [24] and CRESST-III [25]. In the present model the spin-independent (SI) elastic scattering of DM off the normal matter is a t -channel process with the SM Higgs or the singlet scalar as the mediator between the DM and the nucleon. The final formula for the cross sections reads

$$\sigma_{\text{SI}}^p = \frac{\mu_{Xp}^2 m_p^2}{4\pi v_h^2} \alpha_X^2 \sin^2(2\epsilon) \left(\frac{1}{m_h^2} - \frac{1}{m_\phi^2} \right)^2 f_p^2, \quad (14)$$

where m_p is the proton mass, the reduced mass of the proton and DM is $\mu_{Xp} = m_X m_p / (m_X + m_p)$, and the scalar form factor for proton is given by $f_p = 2/9 + 7/9 \sum_{q=u,d,s} f_q^p$, in which $f_u^p = 0.0153$, $f_d^p = 0.0191$ and $f_s^p = 0.0447$ [17]. We probe the parameter space while taking into account bounds from invisible Higgs decay and observed relic density. The ranges of the relevant parameters picked out in our scan are the following: $0.1 < m_{\text{DM}} < 10$ GeV, $0.1 < m_\phi < 10$ GeV, $0.001 < \alpha_X < 1$, and $0 < \sin\epsilon < 0.1$. The model points in the plane $\sigma_{\text{SI}}^p - m_{\text{DM}}$ of Fig. 4 indicate that there are DM masses from 0.2 GeV up to 10 GeV in the viable parameter space. The allowed values for the mixing angle in the respected regions are smaller than $\sim 10^{-4}$ as shown in the right panel of Fig. 4. In the final section we project these same constraints once again.

6 Collider and Beam-dump Bounds

In this section we provide bounds from various experiments when dark particles are engaged in the decay or production at collider or beam-dump experiments.

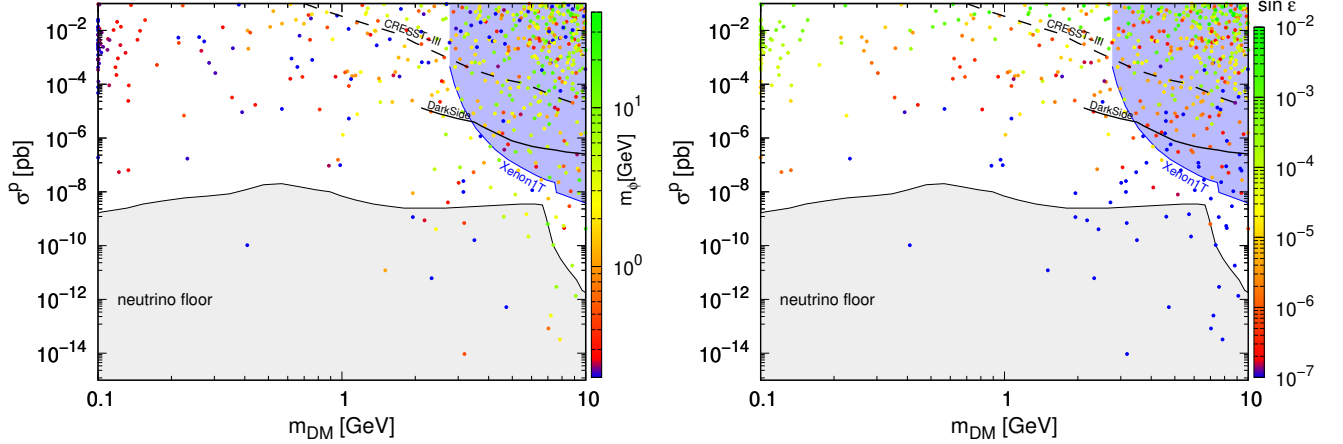


Figure 4: Viable regions are shown after imposing the observed relic density and invisible Higgs decays bounds. The vertical color spectrum shows the singlet scalar mass in the *left* panel and the mixing angle in the *right* panel. Direct detection bounds from Xenon1T, DarkSide50 and CRESST-III are applied.

6.1 Invisible Higgs Decay

In the mass range of interest in this work there are two channels for the SM Higgs invisible decay: $Higgs \rightarrow \phi\phi$ and $Higgs \rightarrow XX$. The invisible Higgs decay width for decay a pair of dark matter is

$$\Gamma_{h \rightarrow XX} = \frac{\alpha_X^2 m_h^3 \sin^2 \epsilon}{16\pi m_X^2} \sqrt{1 - 4(m_X/m_h)^2} [1 - 4(m_X/m_h)^2 + 12(m_X/m_h)^4]. \quad (15)$$

The invisible Higgs decay width for the process $H \rightarrow \phi\phi$ is

$$\Gamma_{h \rightarrow \phi\phi} = \frac{c^2}{8\pi m_h} \sqrt{1 - 4(m_\phi/m_h)^2}, \quad (16)$$

where the couplings c is given by the relation below

$$c = \lambda_{HS} v_h \cos \epsilon + 2\lambda_{HS} v_s \sin \epsilon - 3v_s \lambda_{HS} \sin^3(\epsilon) + 6\lambda_H v_h \sin^2(\epsilon) \cos(\epsilon) - 3\lambda_{HS} v_h \sin^2(\epsilon) \cos(\epsilon) - 6v_s \lambda_S \cos^2(\epsilon) \sin(\epsilon). \quad (17)$$

The measured Higgs mass is $m_h \sim 125.25$ and the total Higgs decay width reads $\Gamma_{\text{Higgs}} = 3.2^{+2.8}_{-2.2}$ MeV [26]. The experimental upper bound on the branching ratio of the invisible Higgs decay at 95% confidence level is $\text{Br}(h \rightarrow \text{invisible}) \lesssim 0.19$ [27]. Thus, the following constraint is applied when the parameter space is scanned

$$\frac{\Gamma_{h \rightarrow XX} + \Gamma_{h \rightarrow \phi\phi}}{\Gamma_{\text{Higgs}}} \lesssim 0.19. \quad (18)$$

6.2 Singlet Scalar Decay

Since the singlet scalar mass varies in the range ($\sim 0.1 - 10$) GeV, when $m_\phi > 2m_f$ it can decay to the SM fermions by the following decay width

$$\Gamma(\phi \rightarrow f^+ f^-) = \frac{N_c^2 m_\phi m_f^2 \sin^2(\epsilon)}{8\pi v_h^2} \left(1 - \frac{4m_f^2}{m_\phi^2}\right)^{3/2}, \quad (19)$$

The total decay width is $\Gamma = \sum_f \Gamma(\phi \rightarrow f^+ f^-)$, and the corresponding life time of the scalar is $\tau = \Gamma^{-1}$. Note that the decay $\phi \rightarrow XX$ is kinematically open when $m_\phi > 2m_X$. The decay width is obtained as

$$\Gamma(\phi \rightarrow XX) = \frac{\alpha_X^2 m_\phi^3 \cos^2 \epsilon}{16\pi m_X^2} \sqrt{1 - 4(m_X/m_\phi)^2} [1 - 4(m_X/m_\phi)^2 + 12(m_X/m_\phi)^4]. \quad (20)$$

The hadronic decay of the singlet scalar with final states, $\pi\pi$, KK , ..., is also important here and has to be taken into account. The big bang nucleosynthesis (BBN) predicts the light element abundances in agreement with the observation. This puts upper limit on the singlet scalar life time which varies between ~ 0.01 sec to 1 sec, in the scalar mass range $\sim 0.1 - 4$ GeV [28]. This upper bound on the scalar life time will be converted to lower bounds on the mixing angle.

6.3 Mediator Production in e^+e^- and LHC Colliders

Direct production of the dark mediator, ϕ , mixing with the SM Higgs is possible at colliders like LEP through the process $e^+e^- \rightarrow Z \rightarrow \phi Z^*$ [29]. Since the rate of the process is proportional to $\sin^2 \epsilon$, then strong constraint on the mixing angle, ϵ , is expected. However, for mediator mass smaller than 10 GeV, it is found that regions with $\sin \epsilon \gtrsim 0.1$ are excluded [30].

On the other hand, CMS and LHCb in search for a new scalar mediator put constraints on $\sigma_{pp-\phi} \times \text{Br}(\phi \rightarrow \mu^+ \mu^-)$ at $\sqrt{s} = 7$ and 8 TeV, respectively [31, 32]. It turns out that the LHC bounds are stronger than that of LEP for scalar mass smaller than about 5 GeV.

6.4 Rare Decays

The relevant rare decays are Υ decay and flavor changing decay of B and K mesons. In these processes the singlet scalar can act as a mediator. The most important decay channel of Υ studied by BaBar is $\Upsilon \rightarrow \gamma \phi^*$, where ϕ decays hadronically to jets [33]. LHCb provides us constraints on two B meson decays, $B^0 \rightarrow K^{*0} \mu^+ \mu^-$ and $B^+ \rightarrow K^+ + \mu^+ \mu^-$, where in both decays the scalar mediator ϕ is decaying to a dilepton [34, 35]. When the scalar mass is below a few hundred of MeV, rare kaon decays become important. Constraints on the mixing angle in terms of the scalar mass can be obtained from the decay $K_L \rightarrow \pi^0 \mu^+ \mu^-$ performed by KTeV experiment [36] and the search for the decay $K^+ \rightarrow \pi^+ \bar{\nu} \nu$ by E949 experiment [37].

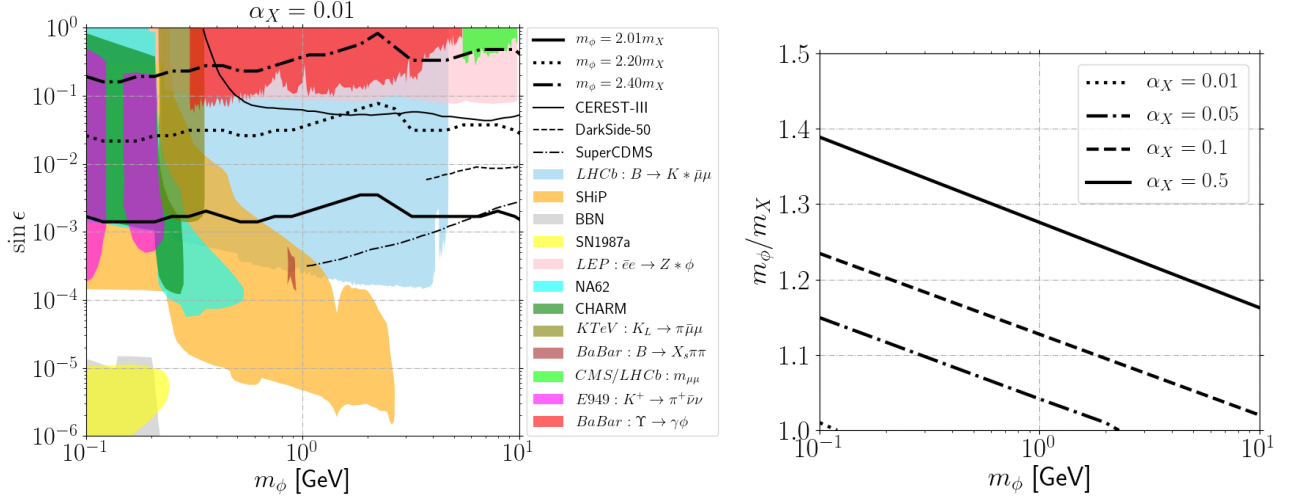


Figure 5: (left) Overlaid of predictions in the resonance region (black tick curves) with constraints by experiments and future projections. (right) Points fulfilling the correct relic abundance by the forbidden mechanism, for α_X values specified in the plot.

6.5 Beam Dump Experiments

We apply bounds from three beam dump experiments at CERN SPS using a 400 GeV proton beam, see [30] and references therein. 1) CHARAM experiments being sensitive to leptonic final states was operating in 1980s. 2) NA62 in dump mode which is an upcoming run and as CHARAM is sensitive to higher scalar mass. 3) SHiP is a planned experiment which will cover a large region of the parameter space not accessible in all earlier experiments.

7 Results

For the resonance case, collider constraints results to be too strong, in such a way that most of the region is excluded by them, even for the case in which the mixing angle ϵ is too small. This can be seen on the left plot of Fig. 5, where we have overlaid the predictions of the model with the tick black curves for different mass shift of the singlet scalar and the DM mass. In particular, provided the mass shift is too small (solid black tick curve), the mixing angle tend to be reduced, but even in this case B meson decay measurements at LHCb results to be strong. Masses for the new particles above 4 - 5 GeV are not constrained yet by the latter experiment, although future direct detection experiments such as SuperCDMS or DarkSide-50 will be able to test this region. The very low mass region, ~ 0.1 GeV is also viable in some discrete range of masses, and experiments such as SHiP or CHARM could explore these parameter space. The forbidden DM relic abundance is dependent only on three parameters: m_X, m_ϕ and α_X . In order to exemplify the relation of them fulfilling the observed relic abundance, in Fig. 5(right)

we show some results obtained with MicrOMEGAS in the mass plane for different values of α_X . This behavior is understood by the interplay between the parameters such that the relic is kept constant [18]. Note that too small α_X requires a too high degeneracy between the new components of the new sector, and a very limited range of masses. These results are in agreement with the scalar version of this model [14]. Since the relic abundance produced by the forbidden channel does not require any particular value of ϵ , one can arbitrarily take too small values of it in such a way to avoid all the constraints and projections from above shown in Fig. 5, then entering into the white region of Fig. 5(left). However, two constraints from too small values of ϵ must be taken into account: BBN and the thermalization of both sectors.

8 Conclusions

In this work we reconsidered the Higgs portal $U(1)_X$ vector dark matter model regarding the low mass of the DM candidate and the singlet scalar. This region of the parameter space with m_{DM} below 10 GeV is not fully investigated in earlier works. In this region of the parameter space we must consider DM annihilation in forbidden channels and near the pole in order to satisfy the observed relic density and CMB bounds. The invisible Higgs decay bounds become strong and to respect the corresponding limits, quite small mixing angle is demanded. Other collider searches in B and K meson are considered along with the limits from beam-dump experiments. Since the singlet scalar can decay to the SM leptons we ensured that it will not spoil the BBN. Our main results given in Fig. 5 concern the viable regions respecting all the theoretical and experimental constraints. We found that when the DM annihilations are near the pole resonance, various parameter space regions result to be excluded, and in the future direct detection constraints will be able to probe most of the region of DM masses $\mathcal{O}(1)$ GeV, whereas lower masses will be tested by experiments such as SHiP and CHARM. On the other hand, regarding the forbidden dark matter production, it shows that as it is independent on the mixing angle ϵ , it is less constrained than the parameter space originated by the resonance production, therefore being more challenging to test regions with such small ϵ .

Note added: while our work was being completed, the article [38] was published on the ArXiv, presenting some overlapping.

9 Acknowledgments

B.D.S has been founded by ANID (ex CONICYT) Grant No. 74200120.

10 Appendix: DM Annihilation Cross Sections

Dark matter annihilation cross sections times the relative velocity are provided in this section. The first formula is the annihilation of DM to a fermion pair being a s -channel process:

$$\sigma_{\text{anni}} v_{\text{rel}}(XX \rightarrow f^+ f^-) = \frac{N_c m_f^2 w^2 \alpha_X^4 \sin^2(2\epsilon)}{36\pi^2 v_h^2} (1 - 4m_f^2/s)^{3/2} \left[\frac{1}{(s - m_\phi^2)^2} - \frac{1}{(s - m_h^2)^2} \right]^2, \quad (21)$$

where N_c is number of colors. The next formula belongs to the DM annihilation to a pair of singlet scalars in s -, t - and u -channel:

$$\begin{aligned} \sigma_{\text{anni}} v_{\text{rel}}(XX \rightarrow ss) = & \frac{\sqrt{1 - 4m_s^2/s}}{32\pi^2 s} \int d\Omega \left[\frac{8}{9} \cos^4(\epsilon) \alpha_X^4 + \frac{64}{9} \cos^4(\epsilon) w^4 \alpha_X^8 \left(\frac{1}{t - m_X^2} + \frac{1}{u - m_X^2} \right)^2 \right. \\ & + 8w^2 \alpha_X^4 \left(\frac{c_1 \cos(\epsilon)}{s - m_\phi^2} - \frac{c_2 \sin(\epsilon)}{s - m_h^2} \right)^2 - \frac{64}{9} \cos^4(\epsilon) w^2 \alpha_X^6 \left(\frac{1}{t - m_X^2} + \frac{1}{u - m_X^2} \right) \\ & - \frac{16c_1 \cos^3(\epsilon) w \alpha_X^4}{3(s - m_X^2)} + \frac{16c_2 \cos^2(\epsilon) \sin(\epsilon) w \alpha_X^4}{9(s - m_h^2)} \\ & + \frac{64c_1 \cos^3(\epsilon) w^3 \alpha_X^6}{3(s - m_\phi^2)} \left(\frac{1}{t - m_X^2} + \frac{1}{u - m_X^2} \right) \\ & \left. - \frac{64c_2 \cos^2(\epsilon) \sin(\epsilon) w^3 \alpha_X^6}{9(s - m_h^2)} \left(\frac{1}{t - m_X^2} + \frac{1}{u - m_X^2} \right) \right], \end{aligned} \quad (22)$$

where, the couplings c_1 is

$$c_1 = 2v_h \lambda_H \sin^3(\epsilon) + w \lambda_{HS} \cos(\epsilon) \sin^2(\epsilon) + 2w \lambda_S \cos^3(\epsilon), \quad (23)$$

and the couplings c_2 is

$$\begin{aligned} c_2 = & v_h \lambda_{HS} \cos(\epsilon) + 2w \lambda_{HS} \sin(\epsilon) - 3w \lambda_{HS} \sin^3(\epsilon) + 6v_h \lambda_H \cos(\epsilon) \sin^2(\epsilon) \\ & - 3v_h \lambda_{HS} \cos(\epsilon) \sin^2(\epsilon) - 6w \lambda_S \cos^2(\epsilon) \sin(\epsilon). \end{aligned} \quad (24)$$

References

- [1] G. Steigman and M. S. Turner, ‘‘Cosmological constraints on the properties of weakly interacting massive particles,’’ *Nuclear Physics B* **253** (1985) 375–386.
- [2] G. Arcadi, M. Dutra, P. Ghosh, M. Lindner, Y. Mambrini, M. Pierre, S. Profumo, and F. S. Queiroz, ‘‘The waning of the WIMP? A review of models, searches, and constraints,’’ *Eur. Phys. J. C* **78** no. 3, (2018) 203, [arXiv:1703.07364 \[hep-ph\]](#).
- [3] L. Bergström, ‘‘Nonbaryonic dark matter: Observational evidence and detection methods,’’ *Rept. Prog. Phys.* **63** (2000) 793, [arXiv:hep-ph/0002126](#).

- [4] G. Arcadi, A. Djouadi, and M. Kado, “The Higgs-portal for dark matter: effective field theories versus concrete realizations,” *Eur. Phys. J. C* **81** no. 7, (2021) 653, [arXiv:2101.02507 \[hep-ph\]](#).
- [5] O. Lebedev, H. M. Lee, and Y. Mambrini, “Vector Higgs-portal dark matter and the invisible Higgs,” *Phys. Lett. B* **707** (2012) 570–576, [arXiv:1111.4482 \[hep-ph\]](#).
- [6] S. Baek, P. Ko, W.-I. Park, and E. Senaha, “Higgs Portal Vector Dark Matter : Revisited,” *JHEP* **05** (2013) 036, [arXiv:1212.2131 \[hep-ph\]](#).
- [7] Y. Farzan and A. R. Akbarieh, “VDM: A model for Vector Dark Matter,” *JCAP* **10** (2012) 026, [arXiv:1207.4272 \[hep-ph\]](#).
- [8] S. Glaus, M. Mühlleitner, J. Müller, S. Patel, and R. Santos, “Electroweak Corrections to Dark Matter Direct Detection in a Vector Dark Matter Model,” *JHEP* **10** (2019) 152, [arXiv:1908.09249 \[hep-ph\]](#).
- [9] G. Arcadi, C. Gross, O. Lebedev, S. Pokorski, and T. Toma, “Evading Direct Dark Matter Detection in Higgs Portal Models,” *Phys. Lett. B* **769** (2017) 129–133, [arXiv:1611.09675 \[hep-ph\]](#).
- [10] G. Arcadi, A. Djouadi, and M. Kado, “The Higgs-portal for vector dark matter and the effective field theory approach: A reappraisal,” *Phys. Lett. B* **805** (2020) 135427, [arXiv:2001.10750 \[hep-ph\]](#).
- [11] K. Ghorbani, “Light vector dark matter with scalar mediator and muon $g-2$ anomaly,” *Phys. Rev. D* **104** no. 11, (2021) 115008, [arXiv:2104.13810 \[hep-ph\]](#).
- [12] M. Duch, B. Grzadkowski, and M. McGarrie, “A stable Higgs portal with vector dark matter,” *JHEP* **09** (2015) 162, [arXiv:1506.08805 \[hep-ph\]](#).
- [13] S. Yaser Ayazi and M. Hosseini, “W boson mass anomaly and vacuum structure in vector dark matter model with a singlet scalar mediator,” [arXiv:2206.11041 \[hep-ph\]](#).
- [14] T. Hara, S. Kanemura, and T. Katayose, “Is light thermal scalar dark matter possible?,” *Phys. Rev. D* **105** no. 3, (2022) 035035, [arXiv:2109.03553 \[hep-ph\]](#).
- [15] R. K. Leane, T. R. Slatyer, J. F. Beacom, and K. C. Y. Ng, “GeV-scale thermal WIMPs: Not even slightly ruled out,” *Phys. Rev. D* **98** no. 2, (2018) 023016, [arXiv:1805.10305 \[hep-ph\]](#).
- [16] A. Semenov, “LanHEP: A Package for the automatic generation of Feynman rules in field theory. Version 3.0,” *Comput. Phys. Commun.* **180** (2009) 431–454, [arXiv:0805.0555 \[hep-ph\]](#).

- [17] G. Belanger, F. Boudjema, A. Pukhov, and A. Semenov, “micrOMEGAs_3: A program for calculating dark matter observables,” *Comput. Phys. Commun.* **185** (2014) 960–985, [arXiv:1305.0237 \[hep-ph\]](#).
- [18] R. T. D’Agnolo and J. T. Ruderman, “Light Dark Matter from Forbidden Channels,” *Phys. Rev. Lett.* **115** no. 6, (2015) 061301, [arXiv:1505.07107 \[hep-ph\]](#).
- [19] **Planck** Collaboration, N. Aghanim *et al.*, “Planck 2018 results. VI. Cosmological parameters,” *Astron. Astrophys.* **641** (2020) A6, [arXiv:1807.06209 \[astro-ph.CO\]](#). [Erratum: *Astron. Astrophys.* 652, C4 (2021)].
- [20] **WMAP** Collaboration, G. Hinshaw *et al.*, “Nine-year wilkinson microwave anisotropy probe (wmap) observations: Cosmological parameter results,” *Astrophys.J.Suppl.* **208** (2013) 19, [arXiv:1212.5226 \[astro-ph\]](#).
- [21] T. R. Slatyer, “Indirect dark matter signatures in the cosmic dark ages. I. Generalizing the bound on s-wave dark matter annihilation from Planck results,” *Phys. Rev. D* **93** no. 2, (2016) 023527, [arXiv:1506.03811 \[hep-ph\]](#).
- [22] K. Griest and D. Seckel, “Three exceptions in the calculation of relic abundances,” *Phys. Rev. D* **43** (1991) 3191–3203.
- [23] **XENON** Collaboration, E. Aprile *et al.*, “Light Dark Matter Search with Ionization Signals in XENON1T,” *Phys. Rev. Lett.* **123** no. 25, (2019) 251801, [arXiv:1907.11485 \[hep-ex\]](#).
- [24] **DarkSide** Collaboration, P. Agnes *et al.*, “Constraints on Sub-GeV Dark-Matter–Electron Scattering from the DarkSide-50 Experiment,” *Phys. Rev. Lett.* **121** no. 11, (2018) 111303, [arXiv:1802.06998 \[astro-ph.CO\]](#).
- [25] **CRESST** Collaboration, A. H. Abdelhameed *et al.*, “First results from the CRESST-III low-mass dark matter program,” *Phys. Rev. D* **100** no. 10, (2019) 102002, [arXiv:1904.00498 \[astro-ph.CO\]](#).
- [26] **Particle Data Group** Collaboration, P. A. Zyla *et al.*, “Review of Particle Physics,” *PTEP* **2020** no. 8, (2020) 083C01.
- [27] **CMS** Collaboration, A. M. Sirunyan *et al.*, “Search for invisible decays of a Higgs boson produced through vector boson fusion in proton-proton collisions at $\sqrt{s} = 13$ TeV,” *Phys. Lett. B* **793** (2019) 520–551, [arXiv:1809.05937 \[hep-ex\]](#).
- [28] A. Fradette and M. Pospelov, “BBN for the LHC: constraints on lifetimes of the Higgs portal scalars,” *Phys. Rev. D* **96** no. 7, (2017) 075033, [arXiv:1706.01920 \[hep-ph\]](#).

- [29] **L3** Collaboration, M. Acciarri *et al.*, “Search for neutral Higgs boson production through the process $e^+ e^- \rightarrow Z^* H_0$,” *Phys. Lett. B* **385** (1996) 454–470.
- [30] M. W. Winkler, “Decay and detection of a light scalar boson mixing with the Higgs boson,” *Phys. Rev. D* **99** no. 1, (2019) 015018, [arXiv:1809.01876 \[hep-ph\]](#).
- [31] **CMS** Collaboration, S. Chatrchyan *et al.*, “Search for a Light Pseudoscalar Higgs Boson in the Dimuon Decay Channel in pp Collisions at $\sqrt{s} = 7$ TeV,” *Phys. Rev. Lett.* **109** (2012) 121801, [arXiv:1206.6326 \[hep-ex\]](#).
- [32] **LHCb** Collaboration, R. Aaij *et al.*, “Search for a dimuon resonance in the Υ mass region,” *JHEP* **09** (2018) 147, [arXiv:1805.09820 \[hep-ex\]](#).
- [33] **BaBar** Collaboration, J. P. Lees *et al.*, “Search for hadronic decays of a light Higgs boson in the radiative decay $\Upsilon \rightarrow \gamma A^0$,” *Phys. Rev. Lett.* **107** (2011) 221803, [arXiv:1108.3549 \[hep-ex\]](#).
- [34] **LHCb** Collaboration, R. Aaij *et al.*, “Search for hidden-sector bosons in $B^0 \rightarrow K^{*0} \mu^+ \mu^-$ decays,” *Phys. Rev. Lett.* **115** no. 16, (2015) 161802, [arXiv:1508.04094 \[hep-ex\]](#).
- [35] **LHCb** Collaboration, R. Aaij *et al.*, “Search for long-lived scalar particles in $B^+ \rightarrow K^+ \chi(\mu^+ \mu^-)$ decays,” *Phys. Rev. D* **95** no. 7, (2017) 071101, [arXiv:1612.07818 \[hep-ex\]](#).
- [36] **KTEV** Collaboration, A. Alavi-Harati *et al.*, “Search for the Decay $K_L \rightarrow \pi^0 \mu^+ \mu^-$,” *Phys. Rev. Lett.* **84** (2000) 5279–5282, [arXiv:hep-ex/0001006](#).
- [37] **BNL-E949** Collaboration, A. V. Artamonov *et al.*, “Study of the decay $K^+ \rightarrow \pi^+ \nu \bar{\nu}$ in the momentum region $140 < P_\pi < 199$ MeV/c,” *Phys. Rev. D* **79** (2009) 092004, [arXiv:0903.0030 \[hep-ex\]](#).
- [38] K.-C. Yang, “Freeze-Out Forbidden Dark Matter in the Hidden Sector in the mass range from sub-GeV to TeV,” [arXiv:2209.10827 \[hep-ph\]](#).